Computer Methods and Programs in Biomedicine 239 (2023) 107623

Contents lists available at ScienceDirect

Computer Methods and Programs in Biomedicine

journal homepage: www.elsevier.com/locate/cmpb

Classification of health deterioration by geometric invariants

Dalibor Cimr[a], Damian Busovsky[a], Hamido Fujita[b,c,d,e,*], Filip Studnicka[a], Richard Cimler[a], Toshitaka Hayashi[a]

[a] Faculty of Science, University of Hradec Kralove, Rokitanskeho 62, Hradec Kralove 50003, Czech Republic
[b] Faculty of Information Technology, HUTECH University, Ho Chi Minh City 700000, Vietnam
[c] Malaysia-Japan International Institute of Technology (MJIIT), Universiti Teknologi Malaysia, Kuala Lumpur 54100, Malaysia
[d] DaSCI Andalusian Institute of Data Science and Computational Intelligence, University of Granada, Granada, Spain
[e] Regional Research Center, Iwate Prefectural University, Iwate 0200611, Japan

ARTICLE INFO

Article history:
Received 28 March 2023
Revised 18 May 2023
Accepted 24 May 2023

Keywords:
Deterioration detection
Ballistocardiography
Cartan curvature
Convolutional neural network
Piezoeceramic sensor

ABSTRACT

Background and Objectives: Prediction of patient deterioration is essential in medical care, and its automation may reduce the risk of patient death. The precise monitoring of a patient's medical state requires devices placed on the body, which may cause discomfort. Our approach is based on the processing of long-term ballistocardiography data, which were measured using a sensory pad placed under the patient's mattress.

Methods: The investigated dataset was obtained via long-term measurements in retirement homes and intensive care units (ICU). Data were measured unobtrusively using a measuring pad equipped with piezoceramic sensors. The proposed approach focused on the processing methods of the measured ballistocardiographic signals, Cartan curvature (CC), and Euclidean arc length (EAL).

Results: For analysis, 218,979 normal and 216,259 aberrant 2-second samples were collected and classified using a convolutional neural network. Experiments using cross-validation with expert threshold and data length revealed the accuracy, sensitivity, and specificity of the proposed method to be 86.51

Conclusions: The proposed method provides a unique approach for an early detection of health concerns in an unobtrusive manner. In addition, the suitability of EAL over the CC was determined.

1. Introduction

Patient deterioration is the significant degradation of the physical state of a hospitalized patient, which can often result in morbidity and/or mortality [23]. The symptoms of deterioration may vary. Some patients may experience a decreased cardiac index followed by decreased blood pressure, tachycardia, and reduced blood flow [8]. As mentioned in [28], before the loss of the electrocardiogram (ECG) signal of dying elderly patients, the P-wave was undetectable in the majority of the observed cases. Prolongation of the corrected time interval between the Q and T peaks of the ECG (QTc) is associated with an increased risk of sudden cardiac death (SCD) [34]. Here the QTc interval is a number calculated via different formulae using heart rate or RR intervals, i.e. time intervals between two successive R peaks in an ECG [14]. Additionally, phenomena associated with breathing such as apnea periods, Cheynne–Stokes breathing, and respiration with mandibular movement are also observed [21,24,28]. Moreover, article [21] states that the death rattle and pulselessness of the radial artery are other physical signs that signal impending death.

Recently, various methods have been developed to predict whether a patient's critical condition will worsen. A reliable approach can prevent patient deterioration. This requirement is not only related to the elderly population [28], but also adults [18,29,32] and pediatric patients [7,22]. The predictive methods for this phenomenon differ in terms of input data and processing. Several studies have investigated the changes in ECG of patients. ECG is a non-invasive method for monitoring heart activity over a period. In recent years, the number of portable ECG-measuring devices has increased significantly. Therefore, focusing on processing data of this type is desirable [20]. Acharya et al. [2] first extracted nonlinear features from second-level discrete wavelet transform decomposed ECG signals and subsequently ranked them

* Corresponding author.
E-mail addresses: h.fujita@hutech.edu.vn, HFujita-799@acm.org (H. Fujita).

https://doi.org/10.1016/j.cmpb.2023.107623

using their t-value. Subsequently, the authors formulated and employed an integrated SCD index using highly ranked features to effectively predict SCD four minutes before onset. This research was expanded by Fujita et al [16], who introduced a novel methodology to automatically classify the heart rate variability (HRV) signals of normal and SCD-risk patients. In a study by Acharya et al., ECG signals were used [1]. Herein, the authors used an eleven-layer convolutional neural network model to process 2-second ECG segments to distinguish shockable and non-shockable ventricular arrhythmias. This phenomenon is crucial for increasing the efficacy of defibrillation via automated external defibrillators. Another study by Ebrahimzadeh et al. [15] extracted HRV parameters from ECG to predict SCD. Both nonlinear and time-frequency HRV features were determined. Subsequently, the dimension of the feature space was reduced using feature selection with healthy and SCD-risk patient classification using a multilayer perceptron and K-nearest neighbor neural network. Brufau et al. [6] employed machine learning to create a model to predict patient deterioration. This study aimed to process the laboratory test results, nursing assessments, vital signs, and demographics of patients hospitalized in general care beds, resulting in the development of a specific early warning score (EWS) that accurately predicts acute deterioration. Kirkland et al. [25] investigated the values of the Braden Scale, oxygen saturation, respiratory rate, and shock index using a multivariate regression analysis to determine the clinical variables statistically associated with patient deterioration.

A review of EWSs by Gerry et al. [19] stated that EWSs are widely used as prediction models for patient deterioration. This review noted that many EWSs have methodological weaknesses that may have detrimental effects on patient care. Another review by Mann et al. [27] focused on tools for predicting patient deterioration. It included results from 46 publications, concluding that the literature has not shown that the implementation of the reviewed tools is reproducibly associated with improvements in patient outcomes. Finally, Blackwell [5] studied statistical models for the early detection of patient deterioration in patients hospitalized in cardiac and cardiac surgery wards. This study concluded that no model could be relied upon in all situations.

In branch of deep learning-based disease diagnosis, Muezzinoglu et al. [31] discussed the use of convolutional neural networks (CNNs) for automated brain tumor classification. The authors propose a patch-based deep feature engineering model called PatchResNet to improve classification performance. The model uses three types of patches of different sizes and two layers of a pretrained ResNet50 as feature extractors. Three selectors were used to obtain 18 final feature vectors, and k nearest neighbors and iterative hard majority voting were used for classification. In other brain problematics, Baygin et al. [4] describes a handcrafted model for accurately detecting schizophrenia using EEG signals. The model generates features using a carbon chain pattern (CCP) and an iterative decomposition model, and extracts subbands of the EEG signal using an iterative tunable q-factor wavelet transform (ITQWT) technique. The clinically significant features are selected using iterative neighborhood component analysis (INCA) and classified using k nearest neighbor (kNN) with a 10-fold cross-validation strategy. The iterative weighted majority method is used to obtain the results in multiple channels. Moreover, Kuluozturk et al. [26] presented a study on cough-based disease detection using machine learning. The authors collected a large cough sound dataset comprising four diagnostic categories (Covid-19, heart failure, acute asthma, and healthy), and trained, validated, and tested a novel model for automatic detection. The model includes four components: feature generation using a specifically directed knight pattern (DKP), signal decomposition using four pooling methods, feature selection using iterative neighborhood analysis (INCA), and classification using the k-nearest neighbor (kNN) classifier with ten-fold cross-validation. The study resulted in the selection of ten best feature vectors and elimination of redundant feature vectors using misclassification rates, followed by feature selection using INCA and input to a kNN classifier.

The proposed approach is based on processing the ballistocardiographic (BCG) data obtained from long-term measurements using a sensory pad equipped with piezoceramic sensors placed under the patient's mattress. BCG is an unobtrusive method for studying the vital functions of a subject by recording the recoil movement of the subject's body. The measured movement appears due to the mechanical activity of the heart and large arteries ensuring blood circulation, and in the case of this study, the mechanical activity of the respiratory system. Both phenomena cause the human body to vibrate slightly. These micro-vibrations then reach the sensors placed directly under/on the body of the subject or propagate through the mattress and bed to reach the sensors. BCG investigations may be used to assess the state of the cardiovascular system of a subject. Starr and Wood [33] conducted a study on a group of 211 healthy persons. Investigation of their ballistocardiograms (BCGm) showed considerable variation in amplitude. The authors interpreted this to be due to the differences in the force exerted by the heart during contraction. Subjects with lower exerted heart force later suffered significantly more from cardiac disability, chiefly coronary heart disease and death, than those with higher exerted heart force. Cimr et al. [13] examined the ability of BCG data to detect various breathing disorders using a 9-layer deep convolutional neural network (CNN) with an ECG R-peak as a trigger. This model achieved an accuracy, sensitivity, and specificity of 96.21%, 88.31%, and 98.69%, respectively, highlighting the possibility of it being used as an early warning system for long-term impending problems. In [3], Baker et al. reported a study focusing on their BCGm examination of coronary heart disease. This study found that abnormalities in BCGm appeared more often in subjects with coronary heart disease. Theorell and Rahe [35] examined the medical and psychological data of 36 people who either experienced myocardial infarction and survived or died from it. These data included their ultralow-frequency BCGm. Here, the mean I–J amplitude served as a rough estimate of the maximal force exerted by the heart during contraction. In the case of subjects dying from myocardial infarction, a significant increase in the mean I–J amplitude appeared approximately six months before their death. However, it is imperative to emphasize that the existing literature does not encompass any research that specifically addresses the management of BCG records for terminally ill individuals. Therefore, this article serves to contribute novel insights to this field of study. By delving into previously unexplored territory, it sheds light on an important aspect that has thus far been overlooked by researchers.

Existing literature prior to [11,13] focused on processing differential geometric invariants. The preprocessing of the examined BCG input in terms of calculating its (first) Cartan curvature (CC) preceded the classification. The dataset can be investigated as a set of 12-dimensional discrete time-parameterized curves in Euclidean space (the BCGm were obtained by deploying four triaxial tensometers) using the Frenet–Serret theory [17]. CCs are uniform functions describing the local properties of curves derived from the derivatives of the vectors of the Frenet frame, that is, a group of n orthogonal normalized vectors in the case of a n-dimensional curve (in the case of $n = 3$, the vectors are tangent, normal, and binormal) [17]. The main reason for processing CC is its invariance to isometric transformations (translations, rotations, and reflections) of the Euclidean group $\mathbb{E}(n)$, where CC is independent of the position of the person on the bed. In [12], another differential invariant in BCG data examination, the Euclidean arc length (EAL), was also included in the data processing. The EAL of a time series in a window of a given length is computed as the sum of the lengths of all segments connecting two successive points in that window of

concrete length [17]. It was first used as a trigger for the unobtrusive detection of respiratory disorders. However, subsequent data processing showed that EAL is not only a useful trigger but also a valuable source of information on the vital state of the measured subject. This led us to include both invariants in this study.

Each method of detection or prediction of patient deterioration listed previously has its own weaknesses. Most research on this topic is based on the processing of ECG data. Precise ECG recording requires the attachment of electrodes to specific locations on the patient's body. Usually, these electrodes are connected to the recording device by a wire, making the measurement obtrusive and difficult to perform in the long term, despite wireless ECG recording devices being available. Otherwise, the processing of clinical or demographic data may be burdened by the late provision of information, resulting in a late warning. A literature review shows that there has been no published research examining BCG data a few hours before death, impending patient deterioration, or during death. Therefore, the outcomes of the current study are unprecedented. In continuation of this article, we also present the distinctive BCG dataset that we have collected and analyzed. This dataset comprises death records of 16 subjects, providing valuable and specific information for further investigation. By sharing this dataset, we aim to facilitate future research in this domain, enabling researchers to delve deeper into the implications and insights derived from these records. The inclusion of this dataset contributes to the overall comprehensiveness and reliability of the findings.

In this study, a novel approach for achieving mechanical triggers of patient deterioration is proposed. The core hypothesis is that deterioration causes significant changes in a BCG signal. Death records of the elderly were collected during long-term BCG data collection using measuring pads equipped with piezoceramic sensors. When these data were examined using expert estimates, deterioration was discovered several hours prior to death. While annotating the trigger in the processed dataset, the expert considered the changes in hemodynamics and respiration effort. The literature shows that these phenomena change before death. BCG cannot be described as easily as ECG because BCG does not have a standardized measurement and strongly depends on the position of the patient or the sensor on the bed. Accordingly, the experts used differential geometric invariants (CC and EAL) to annotate the significant changes. These invariants have proven to be robust tools for searching for changes in BCG data. Obtaining CC and EAL while measuring BCG is completely unobtrusive and may be performed in the long term, even in home care. The calculations of CC and EAL and their further processing are described in the following sections.

2. Methods

In the present study, data measurement and preprocessing were germane. The processed dataset was obtained using measuring pads equipped with piezoceramic sensors placed under the patient's mattress, as shown in Fig. 1.

In the case of a 4-sensor pad, the sensors were placed as follows: (i) approximately under the heart, (ii) under the right lunge, on the same level as sensor (i), (iii) under the left hip approximately, at the level of the patient's centroid, and (iv) on the same level under the right hip. By contrast, in 2-sensor pads, only sensors (i) and (iii) were deployed. The person lying on the bed was not connected to any device, and both sensors were placed directly on the measuring pad, making the measurement unobtrusive. The body recoil movement propagated through the mattress, and the measuring pad reached the piezoceramic sensor. The number of sensors used depended on the type of institution. The beds in retirement homes were equipped with only two sensors because the aim of their data processing was to focus on bed presence and client positioning. In contrast, in the ICU, pads with four sensors were installed to record the vital state of the patient more accurately. In the presented approach, the output signals were considered as 2-dimensional discrete curves parameterized by time, in terms of the timestamp of the recorded data, and 4-dimensional discrete curves in the case of the ICU. This perspective allows for the calculation of the differential invariants of the obtained data.

2.1. Data description

The BCG data, whose processing results are presented in this study, consisted of 16 death records. Data were obtained from the piezoceramic sensors used for body microvibration data collection. The sensor sampling frequency was 330 Hz. The lengths of the records differed owing to the different time intervals from the onset of deterioration to death; a detailed explanation is provided in the next section. The patients' sex, age, height, weight, and other descriptors were unknown; however, none significantly affected the differential invariants used for our purposes.

2.2. Classifier input preparation

After an expert qualitative examination of data from several cases, the deterioration of the patient was found to be readable in the measured data by observing a linear decreasing trend in amplitude and irregularities in vital signs. First, the sliding mean of the Euclidean arc length (SEAL) difference with a window length of 1 h was derived to automate the identification of amplitude drop occurrence. SEAL then served as input data for the sliding least square method (SLSM) with a window length of 30 min and an overlap between adjoining segments of 10 min to examine the trend of the signals' amplitude. In contrast, continuous wavelet transform (CWT) was used to evaluate the data in terms of anomalies in vital signs. The expert subsequently examined sections of the measured data, characterized by a negative trend of SLSM approximation lines, a low difference in the slopes of these lines, a relatively low error of SLSM, and less readable frequencies of vital functions in the output of CWT to annotate the start of deterioration. The SEAL and SLSM lines of a recorded death are shown in Fig. 2a. The parameters examined by annotating the start of the deterioration with respect to the decrease in amplitude corresponding to this particular case are presented in Fig. 2b–d. In these figures, death is observed the moment after which our data no longer recorded a legible trace of heart activity. The outputs of the CWT before and after deterioration are shown in Fig. 3a and b.

However, there is a concern that expert annotations are subjective. To address this issue, expert annotation was evaluated using a CNN by analyzing the required trainable parameters to decrease the computational complexity of the system for future applications [10]. The core hypothesis is that the machine-learning model can classify before and after the threshold with high accuracy. For this purpose, the signal is split into training and testing data, as shown in Fig. 4, where the parts near the threshold are used as testing data, and those before (normal) and after (deterioration) are used as training data. This split was created to achieve the same class balance.

Regarding the threshold, 20% of the shorter vectors represented the testing dataset, and the remaining 80% represented the training dataset. An exact-length dataset was created for the second class. Subsequently, the data were separated into vectors of 660 values, which corresponded to a 2-second sample of 330 Hz frequency.

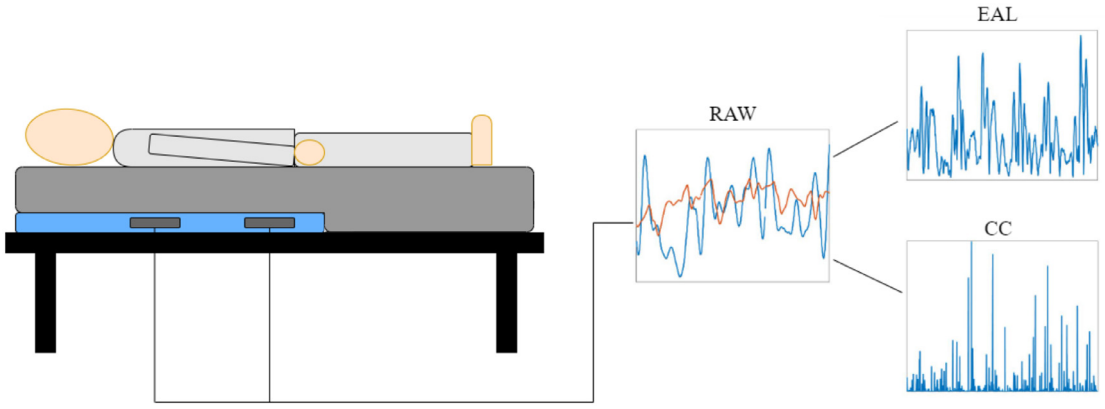

Fig. 1. System architecture.

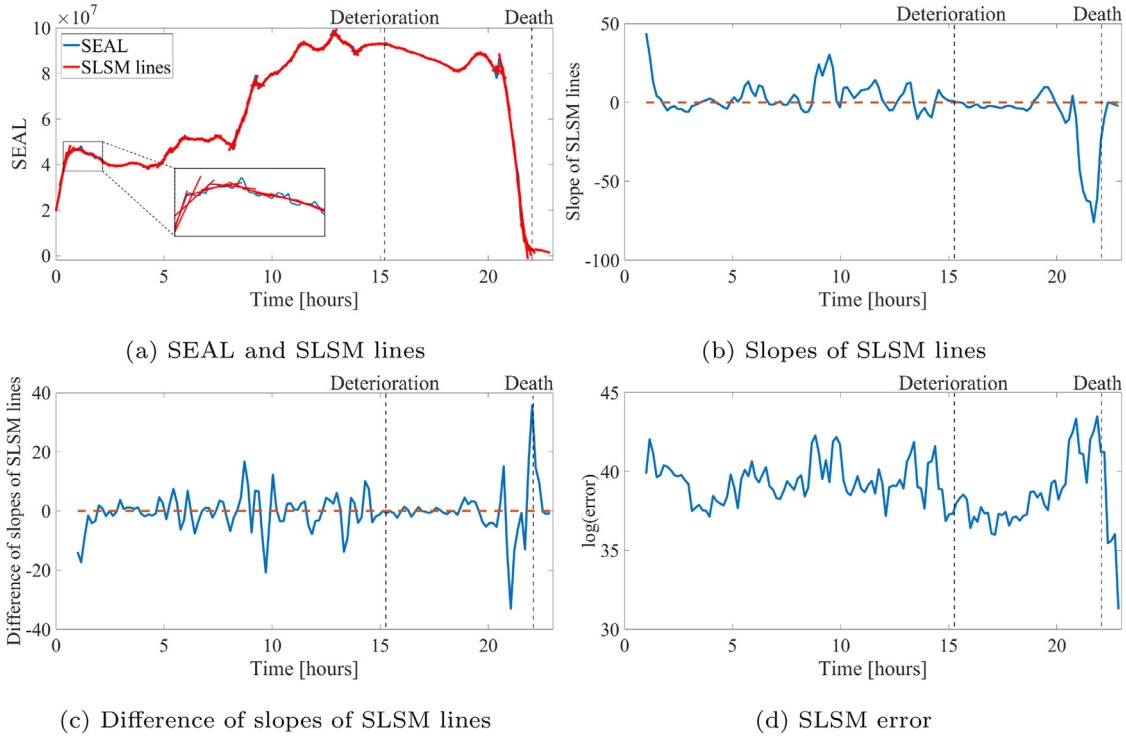

Fig. 2. Expert treshoding.

2.3. Preprocessing

The Euclidean differential invariants are preserved under the actions of the Euclidean group $\mathbb{E}(n)$, rendering them invariant to the position of the person lying on the bed. This is because the cardiovascular system of the person does not change significantly in different positions while lying. Let $\mathbf{C}$ be a matrix whose columns correspond to the signals measured by individual sensors, $\mathbf{C}_i$ be the ith row of $\mathbf{C}$, that is, the vector of measured data corresponding to timestamp $t = t_i$, and $C_{i,j}$ be the element of $\mathbf{C}$ in the ith row and jth column. The nth difference of $\mathbf{C}_i$ can be defined as

$$\mathrm{d}^n\mathbf{C}_i = \sum_{k=0}^{n} (-1)^k \binom{n}{n-k} \mathbf{C}_{i+(n-k)}. \tag{1}$$

Moreover, the first difference of the element $C_{i,j}$ is given by

$$\mathrm{d}C_{i,j} = C_{i+1,j} - C_{i,j}. \tag{2}$$

The EAL of an n-dimensional discrete curve parameterized by time is calculated using the following equation

$$s_m = \sum_{i=1}^{m} \sqrt{\sum_{j=1}^{n} \left(\mathrm{d}C_{i,j}\right)^2}. \tag{3}$$

In (3), s_m represents the EAL of the polyline connecting successive points, starting at the point corresponding to the initial timestamp $t = t_1$ and ending at the point corresponding to the timestamp $t = t_{m+1}$. The elements s_m are stored in the vector $\mathbf{s}$, and the difference $\mathrm{d}\mathbf{s}$ is used for further data processing. However, when calculating the CCs of the processed n-dimensional discrete signal at a given time corresponding to timestamp $t = t_i$, the n orthonormal vectors $\mathbf{e}^q$ and $q \in \{1, 2, \ldots, n\}$ of the relevant Frenet frame must be determined first. This can be achieved using the Gram–Schmidt process [30]. Let the qth vector of the Frenet frame corresponding to the ith row of $\mathbf{C}$ be denoted by $\mathbf{e}_i^q$. Using this notation,

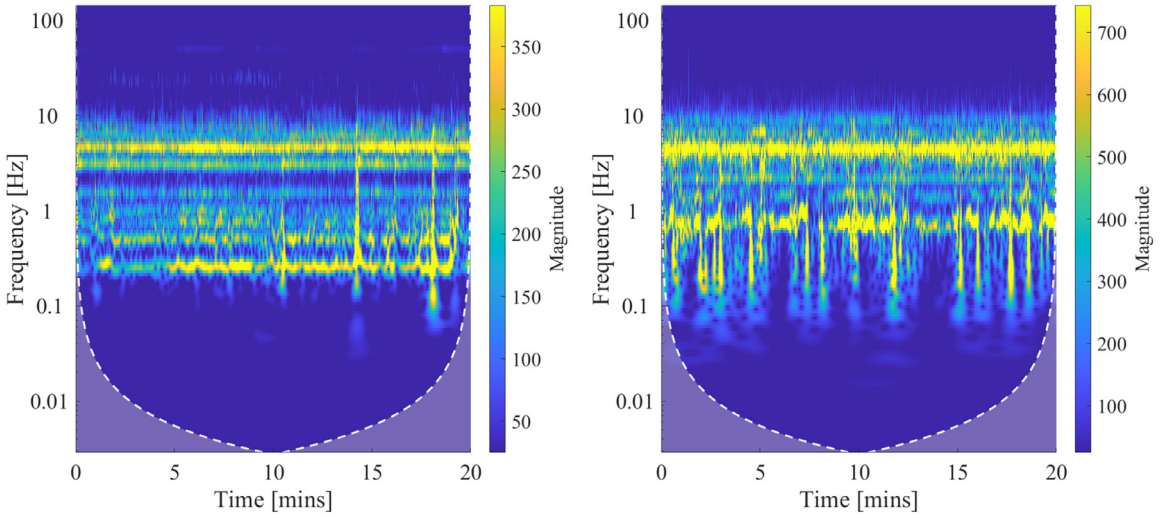

(a) CWT normal (b) CWT after deterioration

Fig. 3. CWT.

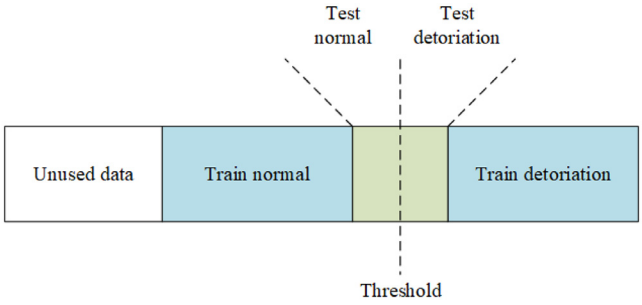

Fig. 4. Data split.

Table 1
The details of the CNN structure with n classes depend on the used dataset.

Layers	Type	No. of output neurons	Kernel size	Stride
0–1	convolution	642 x 30	19	1
1–2	max-pooling	321 x 30	2	2
2–3	convolution	303 x 30	19	1
3–4	max-pooling	151 x 30	2	2
4–5	convolution	141 x 30	11	1
5–6	max-pooling	70 x 30	2	2
6–7	fully connected	30	-	-
6–7	fully connected	20	-	-
7–8	fully connected	2	-	-

all Frenet frame vectors can be determined as follows:

$$\mathbf{e}_i^1 = \frac{\mathrm{d}\mathbf{C}_i}{||\mathrm{d}\mathbf{C}_i||}, \tag{4}$$

$$\mathbf{e}_i^k = \frac{\mathrm{d}^k\mathbf{C}_i - \sum_{j=1}^{k-1}\langle \mathrm{d}^k\mathbf{C}_i, \mathbf{e}_i^j\rangle \mathbf{e}_i^j}{\|\mathrm{d}^k\mathbf{C}_i - \sum_{j=1}^{k-1}\langle \mathrm{d}^k\mathbf{C}_i, \mathbf{e}_i^j\rangle \mathbf{e}_i^j\|}, \quad \text{for } k = 2, 3, \ldots, n-1, \tag{5}$$

$$\mathbf{e}_i^n = \mathbf{e}_i^1 \times \mathbf{e}_i^2 \times \cdots \times \mathbf{e}_i^{n-1}. \tag{6}$$

Here $||\mathbf{v}||$ stands for the Euclidean norm of a vector $\mathbf{v}$, $< \mathbf{u}, \mathbf{v} >$ for the dot product of vectors $\mathbf{u}$ and $\mathbf{v}$, and $\mathbf{u} \times \mathbf{v}$ for the cross product of vectors $\mathbf{u}$ and $\mathbf{v}$. Let

$$\mathrm{d}\mathbf{e}_i^q = \mathbf{e}_{i+1}^q - \mathbf{e}_i^q, \quad \text{for } q = 1, 2, \ldots, n, \tag{7}$$

then, the first CC of the n-dimensional discrete curve at the time corresponding to timestamp $t = t_i$ is given by

$$\kappa_i = \frac{\langle \mathrm{d}\mathbf{e}_i^1, \mathbf{e}_i^2\rangle}{\|\mathrm{d}\mathbf{C}_i\|}. \tag{8}$$

This prescription clearly indicates that an n-dimensional discrete curve may include points for which the first CC cannot be defined owing to division by zero. In our case, this situation occurs when none of the n signals change their values for two consecutive timestamps. From the differential geometry theory perspective, this curve is not *regular*. However, if all sensor values change minimally for two consecutive timestamps, the software used to calculate the CC values may return infinity. In both cases, CC was assigned a value of zero. Two additional facts regarding the introduced invariants must be stated for further processing. First, the denominator in the final prescription of the first CC equals the ith element of difference in the EAL. Second, EAL is more sensitive to signal segments with larger differences and CC, compared to those where the signal locally deviates from the signal's tangents at the previous points. This relates the invariants in a form similar to inverse proportion.

2.4. Model architecture

A unique CNN architecture was developed for classification. The architecture comprised layer blocks formed by convolutional and max-pooling layers. Both block layers slid the input of the previous layer through a window filter defined by the kernel size and stride. Three blocks were provided in the proposed model to obtain the required features from the input data. In all the max-pooling layers, the kernel size for the sliding data was determined by throwing two values with a stride step of two. The first two blocks of the convolutional layers contained a kernel filter comprising 19 vector values, followed by a layer with a filter size of 11. Thirty filters were used in the convolutional layers to determine the patterns with a stride step of one. The design was completed using three successive fully connected layers with 30, 20, and two neurons representing the normal and abnormal classes, as shown in Table 1. The entire architecture contained 91,352 trainable parameters, indicating that an unnecessarily complex model was not required, even for such a large dataset. To avoid overfitting, rectifier linear unit layers were added after each convolutional layer,

and a dropout layer was added between the first and second fully connected layers, all with a value of 0.3. Toward the end of the architecture, a softmax exponential function was used to normalize the findings.

2.5. Limitations and benefits of the approach

Utilizing the 4-sensor BCG pads enables us to acquire long-term measurements for subsequent processing. The data collection procedure itself is non-invasive and non-disruptive to the patients. Simultaneously, the employed measurement method is susceptible to bed movements unrelated to the patient's cardiac activity. Numerous beds in retirement homes are equipped with anti-decubitus mattresses, which induce periodic bed frame movements. However, this signal noise can be easily extracted due to its predictable periodicity. Conversely, movements originating from the patient's skeletal muscles are indistinguishable from the measured data and can introduce inaccuracies in the data classification. Each human body constitutes a unique biological system, and the manifestations of health deterioration may exhibit variations. In this study, a total of 16 death records have been analyzed, which represents a relatively small sample size necessitating expansion for future research endeavors.

The utilization of geometric invariants as an approach in this study is exemplary and builds upon the previous works conducted by the authors. By aggregating the four measured BCG signals into a single time series, we are able to employ the aforementioned Convolutional Neural Network (CNN) described earlier. This technique allows for a comprehensive analysis of the combined data, taking advantage of the rich information encoded in the merged signals. The integration of the geometric invariants and the CNN model enhances the robustness and effectiveness of the analysis, enabling us to extract meaningful insights from the BCG measurements.

2.6. Data availability

The raw BCG data supporting the findings of this study are available in from Mendeley–doi:10.17632/4wrk4fr69w.2. [9].

2.7. Ethics and informed consent

This research was approved by the Committee for Research Ethics of the University of Hradec Králové. The experimental procedure was conducted in accordance with the Ethical Research Framework of the Ministry of Education, Youth, and Sports of the Czech Republic and the ethical requirements of the research. All the participants provided written informed consent to participate in this study.

3. Results

3.1. Experimental setup

As described in Fig. 4, 20% of the shorter vectors around threshold were used as the testing dataset, while the remaining 80% represented the training dataset. The data were separated into vectors of 660 values, which corresponded to a 2-second sample of 330 Hz frequency. An exact-length dataset was created for the second class. The training dataset was then divided into training and validation data by a split of 70% and 30%, respectively. During the training process, 100 epochs were repeated with an early stopping callback when the validation accuracy stopped improving.

Adam optimizer were used to adapt the model attributes. Moreover, the learning rate (LR) value, which represents the size of a step towards minimizing the cost function of a model, was variably reduced for the training process with a patience of five for no decrease in validation loss by a factor of $2 \cdot 10^{-1}$ until the minimum value of $1 \cdot 10^{-5}$. Table 2 summarizes the hyperparameters of the proposed CNN model.

Table 2
Optimization hyperparameters used for training the model.

Input	Optimizer	LR	Patience	Factor	Mini batch	Epochs
660x1	Adam	$1 \cdot 10^{-3}$	$1 \cdot 10^{-5}$	$2 \cdot 10^{-1}$	32	100

Table 3
Confusion matrix description.

O/P	Normal	Abnormal	Acc (%)	Sen (%)	Spec (%)
Normal	TP	FN	$\frac{TP+TN}{TP+TN+FP+FN}$	$\frac{TP}{TP+FN}$	$\frac{TN}{TN+FP}$
Ubnormal	FP	TN		$\frac{TN}{TN+FP}$	$\frac{TP}{TP+FN}$

Table 4
Overall classification of EAL.

Person	Single input			Voting		
ID	Acc (%)	Sen (%)	Spec (%)	Acc (%)	Sen (%)	Spec (%)
0	96.56	94.73	98.55	98.91	97.89	100
1	95.77	97.27	94.36	97.02	100	94.31
2	63.36	70.47	59.91	65.03	80.85	58.62
3	76.80	73.33	81.48	85.71	80.88	92.41
4	80.08	79.76	80.40	90.20	92.55	87.94
5	72.55	94.39	50.71	75	95.18	53.79
6	98.10	96.98	99.28	100	100	100
7	61.44	58.56	67.26	67.31	58.66	90.90
8	95.55	93.80	97.44	99.36	99.69	99.03
9	96.56	94.70	98.59	98.92	97.91	100
10	81.65	91.57	75.55	83.73	95.60	76.66
11	78.39	59.92	96.85	83.21	69.12	97.67
12	72.69	70.17	75.93	87.12	80.00	97.56
13	67.32	65.26	70.03	77.33	75.95	79.09
14	86.20	88.34	84.28	92.00	98.23	86.86
15	74.88	70.16	82.46	83.33	76.74	94.23
Total	81.12	81.21	82.06	86.51	87.45	88.06

At the end, each individual were analyzed on testing dataset to evaluate expert annotations and model performance in detoriation detection. Classification results are evaluated using a tool called a confusion matrix. This matrix tabulates the number of true positives (TP), true negatives (TN), false positives (FP), and false negatives (FN), tabulized in Table 3 with equations for accuracy (Acc), sensitivity (Sen), and specificity (Spec). TP and TN indicate correctly classified normal and abnormal signals, respectively, whereas FP and FN represent the incorrect decisions made by the model.

3.2. Results of the experiments

Table 4 presents the EAL classification results for the proposed system in terms of accuracy, sensitivity, and specificity. The fraction of correct outcomes and all predictions in a testing population is defined as accuracy. It evaluates the dependability of a diagnostic test under given conditions. The proportion of true positives correctly predicted by the classifier is referred to as the sensitivity. It represents the ability of a test to detect a disease. Specificity is defined as the proportion of true negatives correctly predicted by a classifier. This demonstrates the accuracy of a test for predicting normal data.

Each data point around the expert-defined threshold was evaluated separately. Furthermore, sample sequence voting was supplied to improve the system performance, and it succeeded in most cases, except for that of the person with ID 11. Example details for a person with ID 0 are shown in Fig. 5. The green dots represent voting results that result in true-positive or true-negative

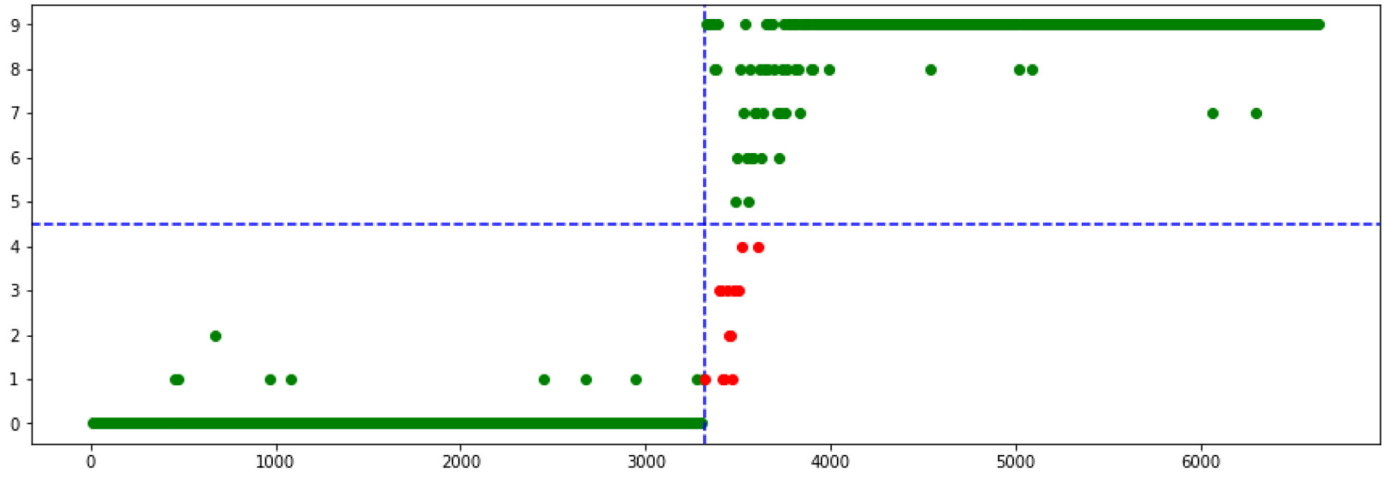

Fig. 5. Testing example for individual patient with ID 0.

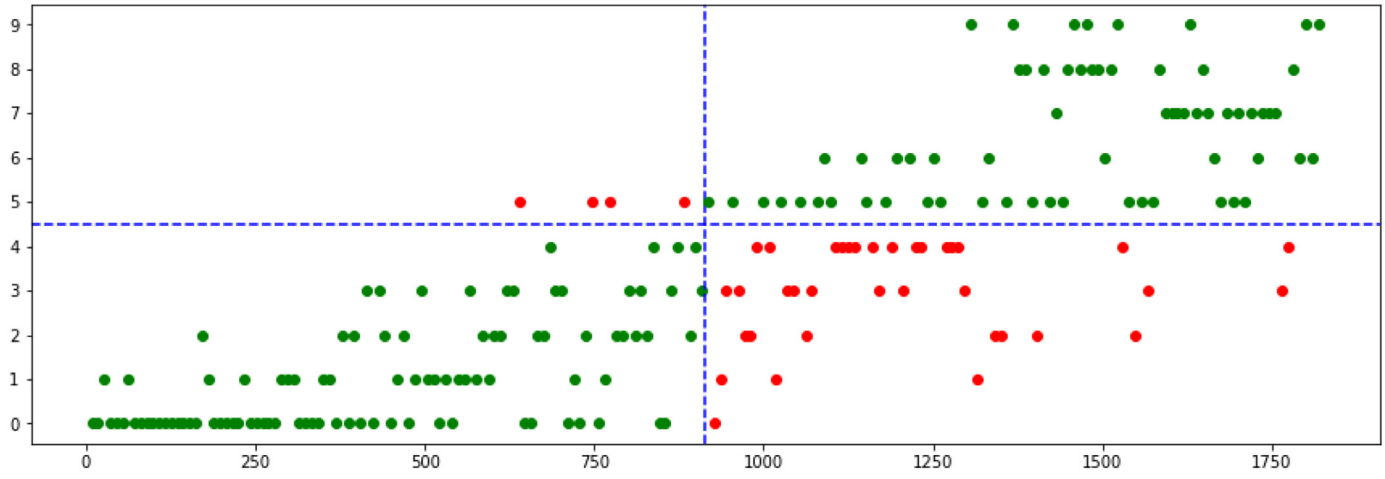

Fig. 6. Testing example for individual patient with ID 12.

decisions, whereas the red dots represent false-positive or false-negative categories. An important aspect of the observation is that most errors are close to the threshold where the patient's condition worsens, without early or late false positives or false negatives. The overall accuracy, sensitivity, and specificity of the proposed technique were 86.51%, 87.45%, and 88.06%, respectively.

Table 5 presents the CC classification results. The differences between individual results with EAL were negligible in terms accuracy, sensitivity, and specificity. However, the sensitivity and specificity for individuals were not balanced. A possible reason is that some CCs were infinite or undefined; these were subsequently replaced with zero. Moreover, the threshold from Section 2.2 was computed from EAL; thus, computing both approaches was not necessary.

Table 5
Overall classification of CC.

Person	Single input			Voting		
ID	Acc (%)	Sen (%)	Spec (%)	Acc (%)	Sen (%)	Spec (%)
0	97.09	99.54	94.63	97.55	99.72	95.36
1	95.46	93.65	97.62	97.02	95.81	98.22
2	59.86	53.67	66.05	61.57	55.37	67.76
3	78.81	89.37	68.24	85.72	93.16	77.64
4	82.52	80.01	85.04	89.97	88.45	91.46
5	69.16	95.55	42.77	66.35	94.91	39.52
6	97.78	99.08	96.49	100	100	100
7	57.23	17.68	96.78	53.81	15.94	95.96
8	97.89	97.95	97.82	99.21	99.21	99.21
9	98.03	99.77	96.28	98.98	99.88	98.07
10	78.52	72.24	84.80	79.63	73.54	85.68
11	79.86	64.93	94.78	85.81	73.92	96.45
12	75.82	83.99	67.65	82.18	88.46	75.51
13	67.45	77.63	57.27	74.73	83.25	65.61
14	86.18	83.09	89.26	92.2	90.24	94.09
15	76.34	86.14	66.53	82.67	90.21	74.62
Total	81.15	80.89	81.37	84.21	83.87	84.69

4. Discussion

The results presented in Tables 4 and 5 are similar owing to the nature of EAL and CC, which was described at the end of Section 2.3. The results of the expert estimation for IDs 0, 1, 6, 8, 9, and 10 indicated immediate health deterioration with high accuracy. This suggests that the system can accurately detect critical patient conditions. However, in case 10, there was a short-term state deterioration in the pre-threshold region, causing the classification accuracy to be lower than that of the other cases with an instantaneous state change.

The condition of patients with IDs 3, 4, and 14 worsened rapidly, although not immediately, within 10 min. This caused

more frequent mispredictions in the near-threshold region, indicating that the system is particularly vulnerable to errors in this area. Therefore, these cases must be focused upon to improve the overall accuracy and reliability of the system. In addition, case 3 was found to have random false positives, which reduced the sensitivity of the system. This is a serious concern because false positives can lead to unnecessary interventions. Such issues must be identified and addressed to optimize the system and minimize the occurrence of false positives while maintaining high sensitivity and accuracy.

Certain findings, however, appeared dubious for persons with IDs 12, 13, and 15, where the model appeared to be ineffective in step threshold cases. Specifically, for ID 12, a detailed qualitative study of the associated RAW data using SEAL, SLSM, and CWT, revealed that the patient's deterioration progressed over a period of 7 h, with accelerated deterioration during the last 2 h. However, an additional examination indicates that a specific trend results in an improvement in the distance from the threshold decision. It may be seen in Fig. 6, the Y-axis shows the number of voting results, indicating that the condition is not acceptable, and the X-axis represents the number of testing samples. This leads to the conclusion that status changes should be gradual rather than stepwise and explains why voting post-processing improved the final prediction. Furthermore, accuracies of 56.45% and 53.48% for the single-input evaluation were unsatisfactory for the situations of IDs 5 and 11, respectively. Examination of the findings revealed a tendency for gradual condition change in distinct timesteps, requiring a double-check of expert design thresholds and performance improvement. Moreover, the individuals with IDs 2 and 7 showed unsatisfactory results. However, after these patients first experienced health-state deteriorations, their SEAL, SLSM, and CWT results improved. After an hour-long increasing trend for SEAL and gradually readable vital function signs in the CWT results, the patients' condition deteriorated again, which culminated in their deaths within approximately 1 h.

Overall, these findings suggest that the system has the potential to accurately detect critical conditions in patients; however, its performance and reliability may be improved.

5. Conclusion

This paper presents a classification model for health deterioration based on geometric invariants. The system operated via BCG sensors placed unobtrusively by measuring pads placed under the patient's mattress. The proposed solution was classified based on CC and EAL preprocessing mechanisms, with data labeling as normal or abnormal based on the SLSM algorithm and CWT. The classifier was designed as an 8-layer deep CNN model for predicting health deterioration. A voting post-processing technique was deployed to improve model performance. Experiments employing cross-validation with an expert threshold and data length demonstrated that the accuracy, sensitivity, and specificity were 86.51%, 87.45%, and 88.06%, respectively.

In future work, the plan is to persist in the collection of long-term BCG data primarily from retirement homes situated in the Czech Republic. The objective is to gather a larger number of death cases for subsequent analysis. Differential geometry provides additional geometric invariants that hold promise for the classification of the measured data, such as affine differential invariants (such as affine arc length and affine curvatures). Furthermore, there is a plan to develop a more resilient algorithm for detecting the threshold of health deterioration. By enhancing the algorithm's robustness, we can improve the accuracy and reliability of identifying critical health changes. These proposed future directions aim to further enhance the understanding and application of BCG measurements in monitoring and predicting health outcomes.

Declaration of Competing Interest

The authors declare no conflicts of interest.

CRediT authorship contribution statement

Dalibor Cimr: Conceptualization, Writing – original draft, Investigation, Data curation, Software. **Damian Busovsky:** Writing – original draft, Investigation, Data curation. **Hamido Fujita:** Writing – review & editing, Supervision. **Filip Studnicka:** Writing – original draft, Investigation, Data curation. **Richard Cimler:** Writing – review & editing, Project administration. **Toshitaka Hayashi:** Conceptualization, Methodology, Writing – original draft, Investigation, Software.

Acknowledgments

The authors are grateful to the Operational Programme "Development of the Internal Grant Agency of the University of Hradec Králové", reg. no. CZ.02.2.69/0.0/0.0/19_073/0016949, project no. IGRA-TYM-2021008 (investigators: Damian Busovsky and Katerina Voglova).

This study was also possible thanks to the project TP01010032 "The Centre of Creative Activities and Knowledge Transfer at University Hradec Kralove." This project was co-financed by the state budget of the Technology Agency of the Czech Republic under the GAMA 2 Progamme.

Furthermore, the authors are grateful to the Excellence project PřF UHK 2215/2023-2024 for its financial support.

References

[1] U.R. Acharya, H. Fujita, S.L. Oh, U. Raghavendra, J.H. Tan, M. Adam, A. Gertych, Y. Hagiwara, Automated identification of shockable and non-shockable life-threatening ventricular arrhythmias using convolutional neural network, Future Gener. Comput. Syst. 79 (2018) 952–959.

[2] U.R. Acharya, H. Fujita, V.K. Sudarshan, V.S. Subbhuraam, L.W.J. Eugene, D.N. Ghista, R.S. Tan, An integrated index for detection of sudden cardiac death using discrete wavelet transform and nonlinear features, Knowl. Based Syst. 83 (2015) 149–158.

[3] B.M. Baker, Ballistocardiography: predictor of coronary heart disease, Circulation 37 (1) (1968) 1–3.

[4] M. Baygin, P.D. Barua, S. Chakraborty, I. Tuncer, S. Dogan, E.E. Palmer, T. Tuncer, A.P. Kamath, E.J. Ciaccio, U.R. Acharya, CCPNet136: automated detection of schizophrenia using carbon chain pattern and iterative TQWT technique with EEG signals, Physiol. Meas. (2023).

[5] J.N. Blackwell, J. Keim-Malpass, M.T. Clark, R.L. Kowalski, S.N. Najjar, J.M. Bourque, D.E. Lake, J.R. Moorman, Early detection of in-patient deterioration: one prediction model does not fit all, Crit. Care Explor. 2 (5) (2020).

[6] S. Romero-Brufau, D. Whitford, M.G. Johnson, J. Hickman, B.W. Morlan, T. Therneau, J. Naessens, J.M. Huddleston, Using machine learning to improve the accuracy of patient deterioration predictions: Mayo clinic early warning score (MC-EWS), J. Am. Med. Inform. Assoc. 28 (6) (2021) 1207–1215.

[7] S.M. Chapman, J. Wray, K. Oulton, M.J. Peters, Systematic review of paediatric track and trigger systems for hospitalised children, Resuscitation 109 (2016) 87–109.

[8] L.-C. Chien, J.Q.K. Lu, C.C.J. Wo, W.C. Shoemaker, Hemodynamic patterns preceding circulatory deterioration and death after trauma, J. Trauma 62 (4) (2007) 928–932.

[9] D. Cimr, D. Bušovský, F. Studnička, H. Fujita, R. Cimler, T. Hayashi, Bcg - patient deterioration impending death, 2023a, Mendeley Data, v2, doi:10.17632/4wrk4fr69w.2.

[10] D. Cimr, H. Fujita, H. Tomaskova, R. Cimler, A. Selamat, Automatic seizure detection by convolutional neural networks with computational complexity analysis, Comput. Methods Programs Biomed. 229 (2023) 107277.

[11] D. Cimr, F. Studnička, Automatic detection of breathing disorder from ballistocardiography signals, Knowl. Based Syst. 188 (2020) 104973.

[12] D. Cimr, F. Studnička, H. Fujita, R. Cimler, J. Šlégr, Application of mechanical trigger for unobtrusive detection of respiratory disorders from body recoil micro-movements, Comput. Methods Programs Biomed. 207 (106149) (2021) 71–86.

[13] D. Cimr, F. Studnička, H. Fujita, H. Tomášková, R. Cimler, J. Kühnová, J. Šlégr, Computer aided detection of breathing disorder from ballistocardiography signal using convolutional neural network, Inf. Sci. (Ny) 541 (2020) 207–217.

[14] P. Dahlberg, U.-B. Diamant, T. Gilljam, A. Rydberg, L. Bergfeldt, QT correction using Bazett's formula remains preferable in long QT syndrome type 1 and 2, Ann. Noninvasive Electrocardiol. 26 (1) (2021).
[15] E. Ebrahimzadeh, F. Fayaz, F. Ahmadi, M.R. Dolatabad, Linear and nonlinear analyses for detection of sudden cardiac death (SCD) using ecg and HRV signals, Trends Res. 1 (2018).
[16] H. Fujita, U.R. Acharya, V.K. Sudarshan, D.N. Ghista, V.S. Subbhuraam, L.W.J. Eugene, J.E.W. Koh, Sudden cardiac death (SCD) prediction based on nonlinear heart rate variability features and SCD index, Appl. Soft Comput. 43 (2016) 510–519.
[17] J. Gallier, Geometric Methods and Applications For Computer Science and Engineering, second ed., Springer, 2011.
[18] H. Gao, A. McDonell, D.A. Harrison, T. Moore, S. Adam, K. Daly, L. Esmonde, D.R. Goldhill, G. Parry, A. Rashidian, C.P. Subbe, S. Harvey, Systematic review and evaluation of physiological track and trigger warning systems for identifying at-risk patients on the ward, Intensive Care Med. 33 (4) (2007) 667–679.
[19] S. Gerry, T. Bonnici, J. Birks, S. Kirtley, P.S. Virdee, P.J. Watkinson, G.S. Collins, Early warning scores for detecting deterioration in adult hospital patients: systematic review and critical appraisal of methodology, BMJ 369 (2020) m1501.
[20] S. Hong, Y. Zhuo, J. Shang, C. Xiao, J. Sun, Opportunities and challenges of deep learning methods for electrocardiogram data: a systematic review, Comput. Biol. Med. 122 (2020) 103801.
[21] D. Hui, R. dos Santos, G.B. Chisholm, S. Bansal, T.B. Silva, K. Kilgore, C.d.S. Crovador, X. Yu, M.D. Swartz, P.E. Perez-Cruz, R.d.A. Leite, M.S.d.A. Nascimento, S. Reddy, F. Seriaco, S. Yennu, C.E. Paiva, R. Dev, S. Hall, J. Fajardo, E. Bruera, Clinical signs of impending death in cancer patients, Oncologist 19 (6) (2014) 681–687.
[22] N. Jacob, Y. Moriarty, A. Lloyd, M. Mann, L. Tume, G. Sefton, C. Powell, D. Roland, R. Trubey, K. Hood, D. Allen, Optimising paediatric afferent component early warning systems: a hermeneutic systematic literature review and model development, BMJ Open 9 (2019) e028796.
[23] D. Jones, I. Mitchell, K. Hillman, D. Story, Defining clinical deterioration, Resuscitation 84 (8) (2013) 1029–1034.
[24] K.A. Kehl, J. Kowalkowski, A systematic review of the prevalence of signs of impending death and symptoms in the last 2 weeks of life, Am. J. Hospice Palliative Med.® 30 (6) (2013) 601–616.
[25] L.L. Kirkland, M. Malinchoc, M.O. O'Byrne, J.T. Benson, D. Kashiwagi, M.C. Burton, P. Varkey, T.I. Morgenthaler, A clinical deterioration prediction tool for internal medicine patients, Am. J. Med. Qual. 28 (2) (2013) 135–142.
[26] M. Kuluozturk, M.A. Kobat, P.D. Barua, S. Dogan, T. Tuncer, R.-S. Tan, E.J. Ciaccio, U.R. Acharya, DKPNet41: directed knight pattern network-based cough sound classification model for automatic disease diagnosis, Med. Eng. Phys. 110 (2022) 103870.
[27] K. Mann, N. Good, F. Fatehi, S. Khanna, V. Campbell, R. Conway, C.M. Sullivan, A. Staib, C. Joyce, D.A. Cook, Predicting patient deterioration: a review of tools in the digital hospital setting, J. Med. Internet Res. 23 (9) (2021) e28209.
[28] K. Matsunami, K. Tomita, H. Touge, H. Sakai, A. Yamasaki, E. Shimizu, Physical signs and clinical findings before death in ill elderly patients, Am. J. Hospice Palliative Med.® 35 (4) (2018) 712–717.
[29] J. McGaughey, F. Alderdice, R. Fowler, A. Kapila, A. Mayhew, M. Moutray, Outreach and early warning systems (EWS) for the prevention of intensive care admission and death of critically ill adult patients on general hospital wards (review), Cochrane Database of Syst. Rev. (2007) CD005529.
[30] F. Milano, The frenet frame as a generalization of the park transform, IEEE Trans. Circuits Syst. I Regul. Pap. (2022) 1–11.
[31] T. Muezzinoglu, N. Baygin, I. Tuncer, P.D. Barua, M. Baygin, S. Dogan, T. Tuncer, E.E. Palmer, K.H. Cheong, U.R. Acharya, PatchResNet: multiple patch division–based deep feature fusion framework for brain tumor classification using MRI images, J. Digit. Imaging (2023) 1–15.
[32] M.E.B. Smith, J.C. Chiovaro, M.E. O'Niel, D. Kansagara, A.R. Quinenos, M. Freeman, M. Motuapuaka, C. Slatore, Early warning system scores for clinical deterioration in hospitalized patients: a systematic review, Ann. Am. Thorac. Soc. 11 (9) (2014) 1454–1465.
[33] I. Starr, F.C. Wood, Twenty-year studies with the ballistocardiograph, Circulation 23 (5) (1961) 714–732.
[34] S.M.J.M. Straus, J.A. Kors, M.L.D. Bruin, C.S.v.d. Hooft, A. Hofman, J. Heeringa, J.W. Deckers, J.H. Kingma, M.C.J.M. Sturkenboom, B.H.C. Sticker, J.C.M. Witteman, Prolonged QTc interval and risk of sudden cardiac death in a population of older adults, J. Am. Coll. Cardiol. 47 (2) (2006) 362–367.
[35] T. Theorell, C.R. Rahe, Life change events, ballistocardiography and coronary death, J. Human Stress. 1 (3) (1975) 18–24.